Supplementary Information

Nitrogen Doped Carbon Materials Derived from Gentiana scabra Bunge as High-performance Catalysts for Oxygen Reduction Reaction

Cancan Wang,[a] Winston Duo Wu,[b] Ying Wang,[c] Dan Xu[a,]* and Feng Yan[a,]*

[a]*Jiangsu Key Laboratory of Advanced Functional Polymer Design and Application, Department of Polymer Science and Engineering, College of Chemistry, Chemical Engineering and Materials Science, Soochow University, Suzhou, 215123, China.*

[b]*Suzhou Key Laboratory of Green Chemical Engineering, School of Chemical and Environmental Engineering,College of Chemistry, Chemical Engineering and Materials Science, Soochow University, Suzhou, 215123, China*

[c]*Analysis Test Centre, Soochow University, Suzhou, 215123, China*

E-mail: fyan@suda.edu.cn; dxu@suda.edu.cn

1. Experimental Section

1.1 Material Characterization

X-ray photoelectron spectra were obtained through an XPS-7000 spectrometer (Rigaku) whose excitation source is Mg Kα radiation. The SEM was carried out by Hitachi Model S-4700 field emission which is attached a spectrometer to complete the EDX measurement. The TEM images were obtained by Tecnai G220 under an acceleration voltage of 160 kV. X-ray powder diffraction was conducted by Philips X'Pert PRO diffractometer equipped with nickel-filtered Cu Kα radiation. Raman spectra were examined with the use of LabRAM HR800 from JY Horibain. Nitrogen sorption isotherms were obtained from ASAP 2020 accelerated surface area and porosimetry instrument, Micromeritics. The apparent surface area was calculated using the Brunauer-Emmett-Teller method at 77 K. The pore size distribution (PSD) plots were obtained from the density functional theory (DFT). The dried Gentiana scabra Bunge was grinded by using a multi-function grinder (BJ-300), produced by Deqingbaijie Limited Co., at the rotation rate of 25000 rpm.

1.2 Electrochemical test

(1) In acid environment (0.5 M H_2SO_4 as the electrolyte), the saturated calomel electrode (SCE) was the reference electrode, and a platinum plate was the counter electrode. All potentials were then converted to be vs RHE referring to the Nernst equation[1]:

$$E_{RHE} = E_{SCE} + 0.059pH + E^0_{SCE}$$

where E_{SCE} is the measured potential, and $E^0_{SCE} = 0.242$ V.

(2) In alkaline environment (0.1 M KOH as the electrolyte), a Hg/HgO reference electrode replaced SCE as the reference electrode. All potentials were then converted to be vs RHE referring to the Nernst equation[2]:

$$E_{RHE} = E_{Hg/HgO} + 0.059pH + E^0_{Hg/HgO}$$

where $E_{Hg/HgO}$ is the measured potential, and $E^0_{Hg/HgO} = 0.098$ V.

(3) The electron transfer number (n) was analyzed by the Koutecky-Levich (K-L) equation:

$$\frac{1}{J} = \frac{1}{J_0} + \frac{1}{J_K} = \frac{1}{B\omega^{1/2}} + \frac{1}{J_K}$$

$$B = 0.62nFC_0(D_0)^{2/3}\nu^{-1/6}$$

Where J, J_L and J_K are the measured current density, the diffusion limiting current density and the kinetic limiting current density, respectively, B is the value of Levich slope, ω is the electrode rotating rate, F is the Faraday's constant, C_O is saturated dissolved concentration of O_2 in the electrolyte, D_O is the diffusion coefficient of oxygen in the electrolyte, and ν is the dynamic viscosity of the electrolyte.

1. Q. Liu, J. Shi, J. Hu, A. M. Asiri, Y. Luo, and X. Sun, *ACS Appl. Mater. Interfaces* 2015, **7**, 3877-3881.
2. J. Zhu, D. Xu, C. Wang, W. Qian, J. Guo, F. Yan, *Carbon* 2017, **115**, 1-10.

2. Additional Material Characterizations

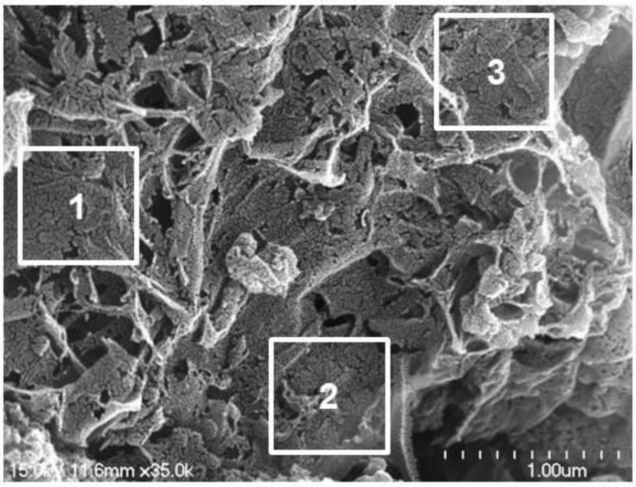

Spot 1		Spot 2		Spot 3	
Element	Weight%	Element	Weight%	Element	Weight%
C K	73.29	C K	70.89	C K	75.47
O K	13.10	O K	12.69	O K	10.12
N K	13.61	N K	16.42	N K	14.41
Fe K	0.00	Fe K	0.00	Fe K	0.00
Total	100.00	Total	100.00	Total	100.00

Fig. S1 Energy dispersive X-ray (EDX) analysis of randomly selected spots of G-N-900-4.

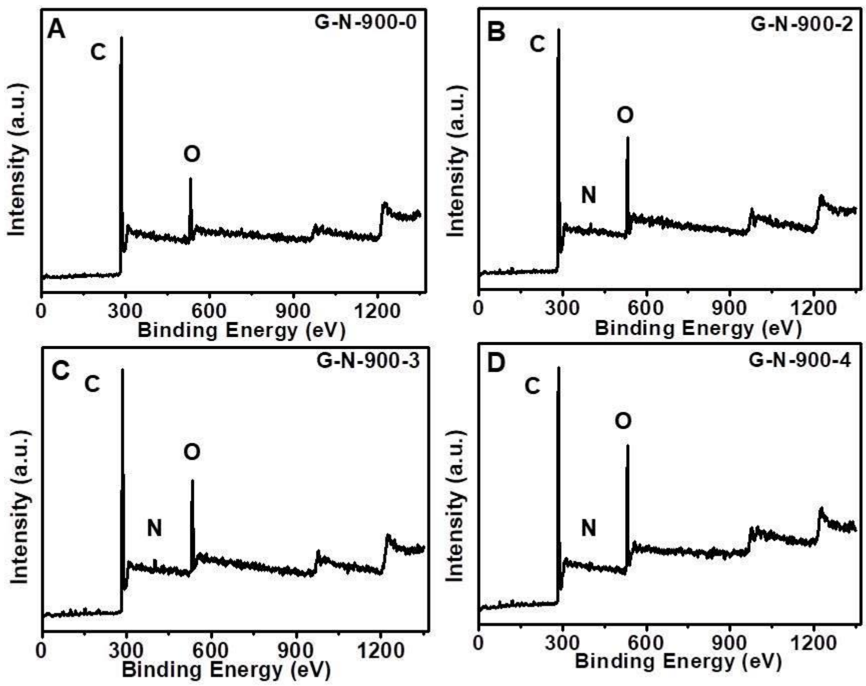

Fig. S2 X-ray photoelectron spectroscopy (XPS) spectrum of G-N-900-0 A); G-N-900-2 B); G-N-900-3 C), and G-N-900-4 D).

Table S1 X-ray photoelectron spectroscopy (XPS) Analysis of G-N-900-n

Samples	XPS (at%)		
	C	N	O
G-N-900-0	86.67	1.7	11.43
G-N-900-2	81.73	2.78	15.49
G-N-900-3	82.57	3.08	14.34
G-N-900-4	79.20	1.15	19.65

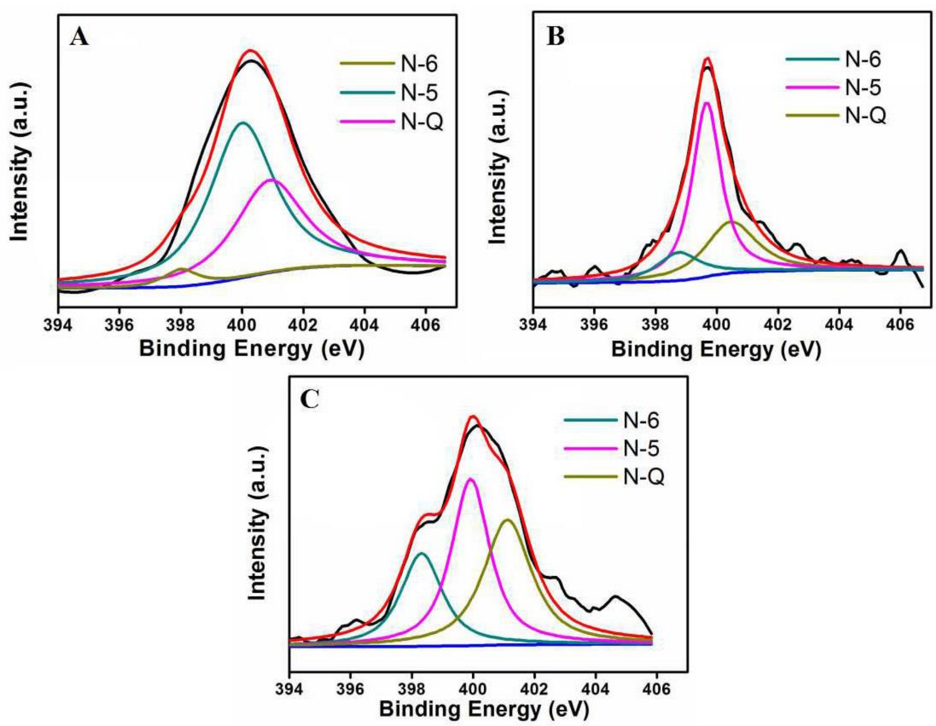

Fig. S3 High resolution N 1s XPS spectra of G-N-900-0 A); G-N-900-2 B); G-N-900-3 C).

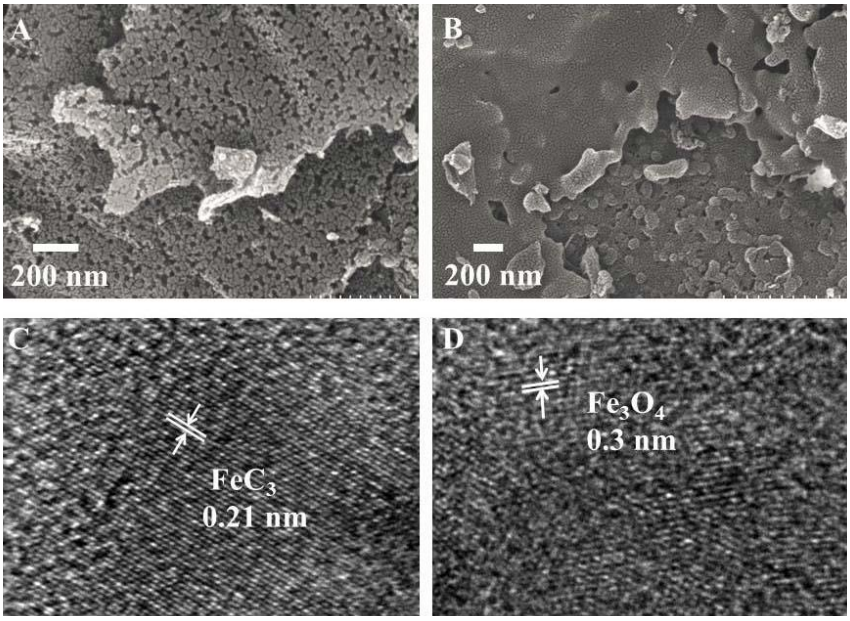

Fig. S4 SEM images of G-N-900-2 (A) and G-N-900-3 (B); High magnificence of HR-TEM images of nanoparticles embedded in G-N-900-4 (C) and (D).

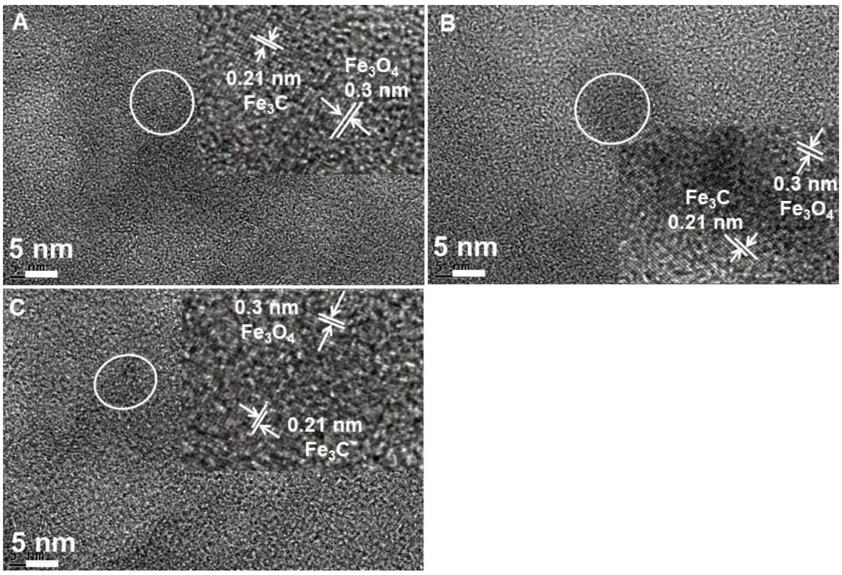

Fig. S5 HR-TEM images of G-N-900-n and nanoparticles embedded in G-N-900-n: G-N-900-0 (A), G-N-900-2 (B) and G-N-900-3 (C)

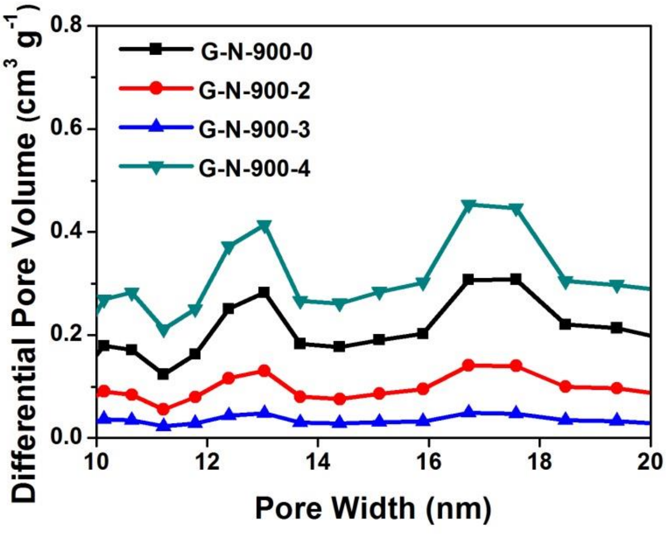

Fig. S6 Pore-size distributions of resultant materials calculated by density function theory method.

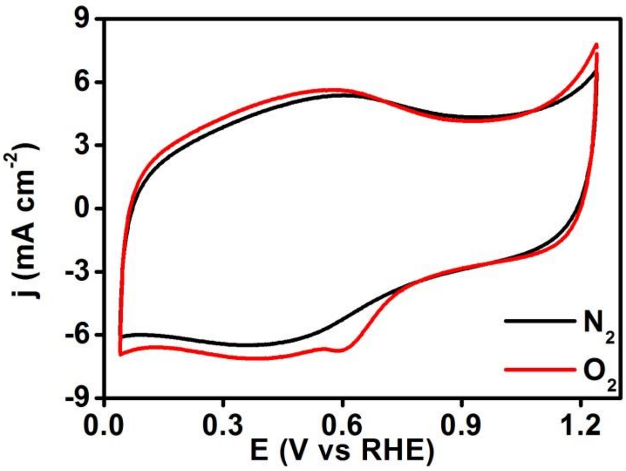

Fig. S7 CV curves of G-N-900-4 in N_2-saturated, O_2-saturated 0.5 M H_2SO_4 solution with a scanning speed of 50 mV s^{-1}.

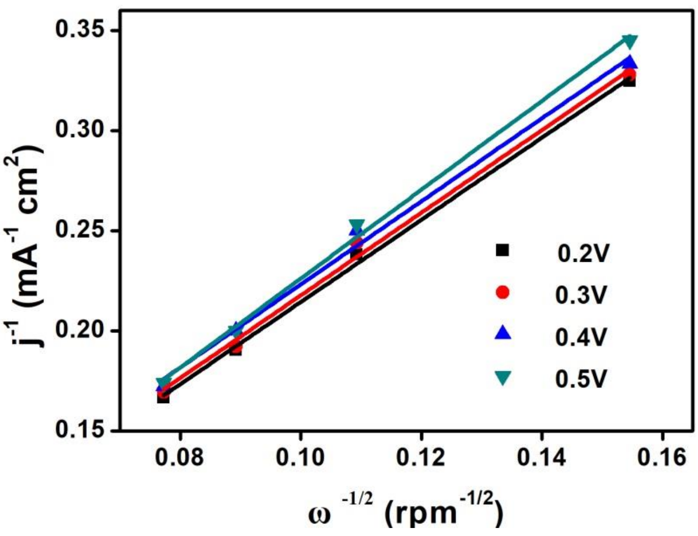

Fig. S8 Koutecky-Levich plots of G-N-900-4 in acid medium at different potentials from 0.2 to 0.5 V.

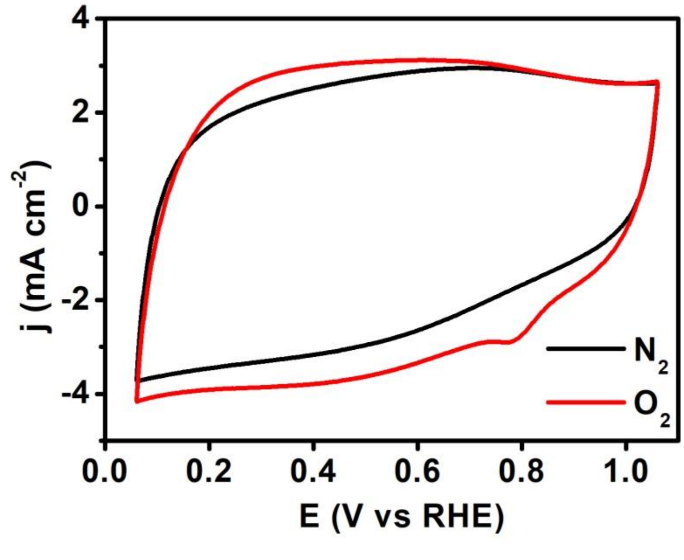

Fig. S9 CV curves of G-N-900-4 in N_2-saturated, O_2-saturated 0.1 M KOH solution with a scanning speed of 50 mV s^{-1}.

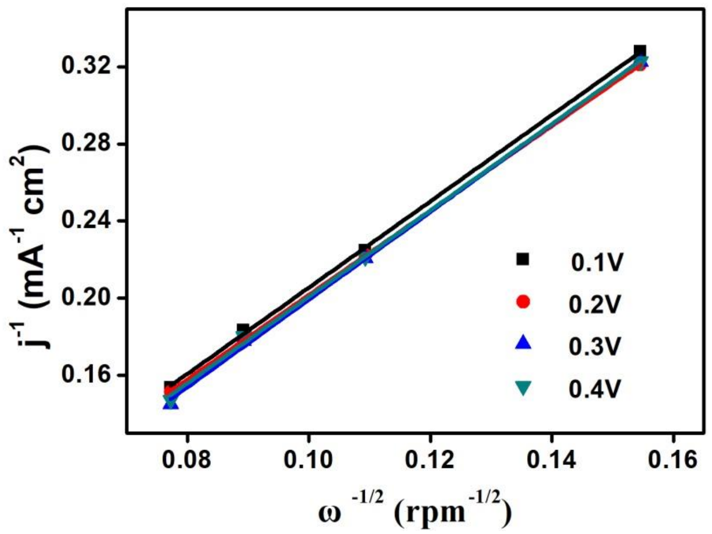

Fig. S10 Koutecky-Levich plots of G-N-900-4 in alkaline medium at different potentials from 0.1 to 0.4 V.

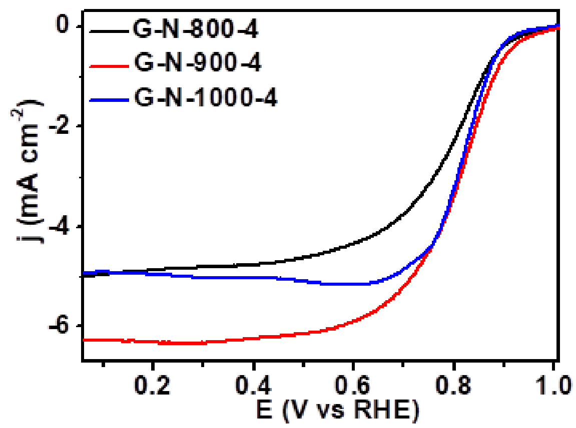

Fig. S11 Rotating disk electrode (RDE) polarization curves of G-N-T-4 in alkaline medium, T: 800, 900 and 1000℃.